Oil Sands: Rock Physics Analysis from Well Data, Alberta, Canada

Sabrina Aliyeva and Jack Dvorkin, Stanford University, Weimin Zhang, Cenovus Energy Inc., Canada.*

Summary

The common properties of bitumen are: high specific gravity, low hydrogen to carbon ratios, high carbon residues, and high contents of asphaltenes, heavy metal, sulphur and nitrogen. Since it is very viscous, it does not flow so easily. Bitumen has gravity of about 10.3 API which translates into its density about 1.3 g/cc.

Bitumen deposits mostly found at very shallow depth, where temperature doesn't exceed 15°C. Therefore in-situ bitumen acts as a solid, since bitumen properties depend on temperature. The less temperature is in a formation the more viscous bitumen is. Hence velocities and modulus of bitumen will also depend on temperature.

Introduction

Bitumen sands are enormous unconventional resource of hydrocarbons. One challenge faced during exploration and monitoring is relating the elastic properties of such sands to their porosity and conditions, namely pressure and temperature.

Laboratory ultrasonic velocity measurements have been conducted on pure bitumen samples as well as bitumen sands (e.g., Wolf, 2010). A big challenge in interpreting such measurements for the purpose of seismic interpretation is the dichotomy between the high frequency of laboratory experiments and relatively low frequency of seismic exploration data and well data. To bridge this difference, experiments have been conducted in the laboratory in the seismic range frequencies (e.g., Das and Batzle, 2008).

Such experiments are fairly complicated. Hence, it is beneficial to examine well data where various sand properties, including density, porosity, and the elastic-wave velocity are available and provide significantly larger number of data points as compared to laboratory data. Here we examine two such well datasets and establish a velocity-porosity model for bitumen sands.

Data Display and Cross Plots

Figures 1 and 2 display the measured data in Well 1 and Well 2, respectively, in the depth interval relevant to the oil sands reservoir. The curves shown in the fourth plot in both figures are for the density-derived (ϕ_ρ), neutron (ϕ_N), and total (ϕ_t) porosity. ϕ_ρ was computed from the bulk density (ρ_b) as

$$\phi_\rho = (2.65 - \rho_b)/1.65, \quad (1)$$

where the density is in g/cc and also it is implicitly assumed that the mineral matrix is pure quartz with density 2.65 g/cc and the pore fluid is water with density 1 g/cc. This is not necessarily the true density of the pore fluid as the density of the bitumen may exceed that of water. However, we still use this equation which gives us a plausible range of porosity.

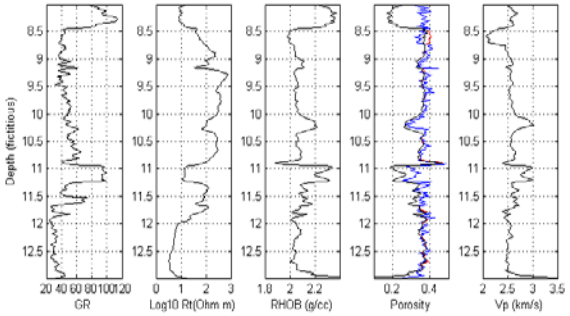

Figure 1. Measured well data versus depth for Well 1. From left to right: gamma ray; true resistivity; bulk density; density-derived (red), neutron (blue), and total (black) porosity; and the P-wave velocity. Depth values are fictitious.

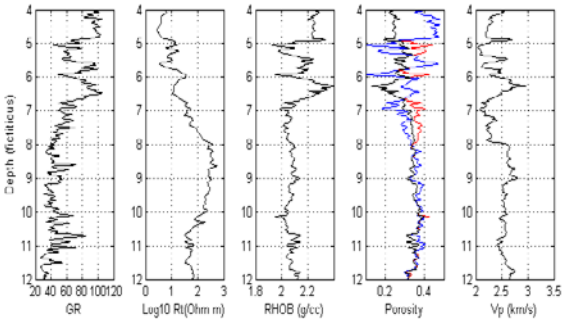

Figure 2. Same as Figure 1 but for Well 2.

Where the ϕ_N values fall below the ϕ_ρ values, we assume that the pore fluid is (at least partially) gas and, hence, compute the total porosity from a commonly used empirical equation as

$$\phi_t = (\phi_\rho + \phi_N)/2. \quad (2)$$

In the rest of the interval we assume $\phi_t = \phi_\rho$. The top portion of the intervals under examination in both wells is

DOI http://dx.doi.org/10.1190/segam2012-0861.1

Oil Sands: Rock Physics Analysis from Well Data

shale with high GR values and ϕ_N strongly exceeding ϕ_ρ. This shale is followed by apparently gas-saturated intervals where ϕ_N is smaller than ϕ_ρ and the P-wave velocity (V_p) is smaller than in the rest of the interval indicating the presence of some gaseous fluid phase. Below the gas-saturated intervals is sand with heavy oil (bitumen). In Well 1 it is followed by the bottom shale interval with relatively high GR. In Well 2 this bottom shale layer is thinner and not as well defined as in Well 1.

In this analysis we concentrate on four depth intervals in the wells under examination representing the top shale, gas sand, oil sand, and bottom shale beneath the oil sand. The depth ranges selected for these facies are listed in Table 1 for Well 1 and Table 2 for Well 2.

Table 1. Four intervals selected in Well 1 and their depth ranges.

Intervals	Depth Range (fictitious)
Top Shale	8.00 – 8.50
Gas Sand	8.50 – 8.75
Oil Sand	8.75 – 10.95
Bottom Shale	10.95 – 11.25

Table 2. Four intervals selected in Well 2 and their depth ranges.

Intervals	Depth Range (fictitious)
Top Shale	4.00 – 4.80
Gas Sand	4.81 – 5.34 5.80 – 6.01 6.65 – 7.80
Oil Sand	7.90– 10.65

In Figures 3 and 4 we cross-plot the P-wave velocity versus the bulk density for Well 1 and Well 2, respectively and color-code the data points by (a) gamma-ray; (b) the difference between the neutron and density porosity, and (c) depth. We observe that the oil sand data points form a tight velocity-density trend which is approximately the same for both wells.

In Figures 5 and 6 we show the velocity-density, velocity-porosity, and GR-porosity cross-plots for both wells, this time color-coded by the facies as listed in Tables 1 and 2. Here we observe that the oil sand clearly separates from the gas sand in the velocity-density and velocity-porosity cross-plots. In the same cross-plots, the top shale appears much softer than the bottom shale in the same density and porosity range. Finally, in the GR versus total porosity cross-plot, we observe a fairly distinct relation between these two parameters: as GR (presumably the clay content) increases, the total porosity decreases.

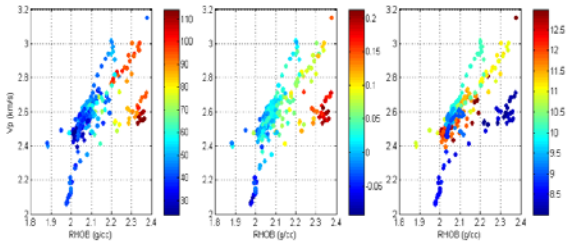

Figure 3. Velocity versus bulk density cross-plots for Well 1. The color-coding from left to right is GR, the difference between the neutron and density porosity, and depth (fictitious).

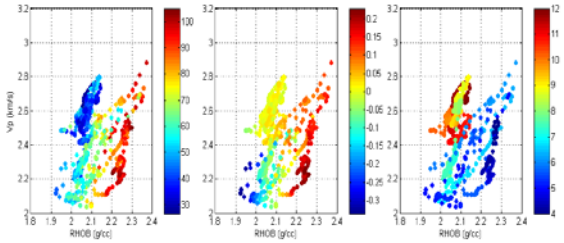

Figure 4. Same as Figure 3 but for Well 2.

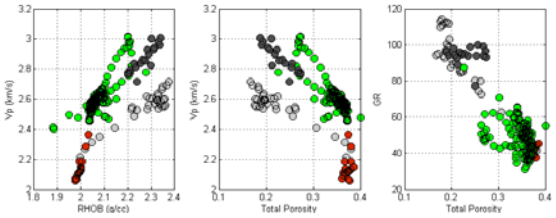

Figure 5. Well 1. Cross-plots with the data color-coded by the four facies listed in Table 1. From left to right: velocity versus density; velocity versus the total porosity; and GR versus the total porosity. Green symbols are for the oil sand; red is for gas sand; light gray is for top shale; while dark-gray is for bottom shale.

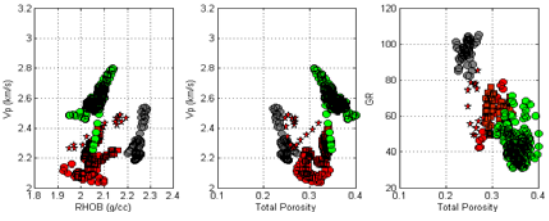

Figure 6. Same as Figure 5 but for Well 2. Different shapes of the red symbols correspond to the three gas sand intervals listed in Table 2.

Finally, in Figure 7 we superimpose the graphs from Figure 6 upon those from Figure 5. Arguably, the most important

DOI http://dx.doi.org/10.1190/segam2012-0861.1

observation from these combined plots is that the oil sand data pairs from both wells fall essentially on top of each other.

The gas sand in Well 2 appears to be different from that in Well 1: it has somewhat larger density and smaller total porosity. One possible reason is that the gas sand in Well 1 appears to be cleaner (have smaller GR and, hence, less clay) than in Well 2 as illustrated by the third plot in Figure 7. Also the top shale in Well 2 appears to have smaller density (and larger porosity) than in Well 1.

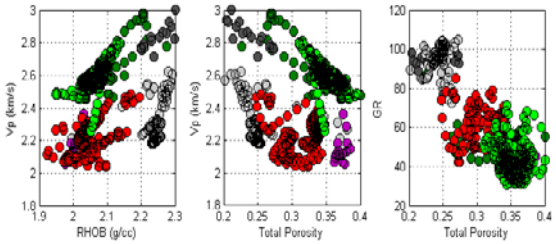

Figure 7. Superposition of plots from Figure 5 and 6. The Well 1 data are shown in darker colors. The bottom shale from Well 1 is shown as black squares. Gas sand in Well 1 is shown as magenta circles.

The differences between the gas sand in Well 1 and Well 2 as well as the differences between the top shale may be related to the depositional differences between the two locations and depths. For now we will concentrate on the rock physics modeling of the oil sand which appears to be similar in both wells.

Rock Physics Modeling of Oil Sand.

To arrive at an appropriate rock physics model, let us assume that the oil sand is a suspension of quartz grains in heavy oil. In such an arrangement, the heavy oil is load-bearing. The lower elastic Hashin-Shtrikman bound has been designed with such geometry in mind. Hence, our first attempt is to model the elastic properties of the oil sand as the lower Hashin-Shtrikman bound of quartz and heavy oil.

The needed elastic moduli and density for quartz are 36.60 GPa for the bulk modulus, 45.00 GPa for the shear modulus, and 2.65 g/cc for the mineral density. To obtain these values for the bitumen, we resort to the experimental results of Wolf (2010) where the bulk and shear moduli were measured versus temperature (Figure 8). The in-situ temperature of the oil sand at the location under investigation is 12^{o} C. The corresponding data point in Figure 8 gives the bulk modulus 2.50 GPa and the shear modulus 0.50 GPa.

The other set of bitumen measurements we use are from Batzle et al. (2004). Here, the bulk modulus of the bitumen at 12^{o} C is 3.50, while the shear modulus is 0.70 GPa.

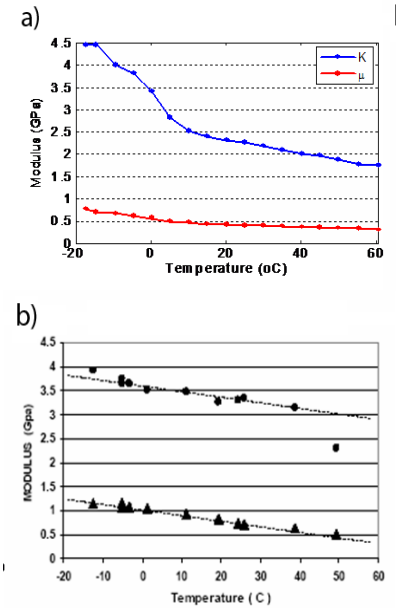

Figure 8. a) Bulk and shear modulus as a function of temperature for the bitumen sample from Wolf (2010); b) bulk and shear modulus of possibly heavier oil as measured by Batzle et al. (2004).

The modeling results shown in Figure 9 for Well 1 and Well 2 indicate a reasonable match between the data and model predictions, although the oil sand data points lie slightly above the lower Hashin-Shtrikman bound (Figure 10).

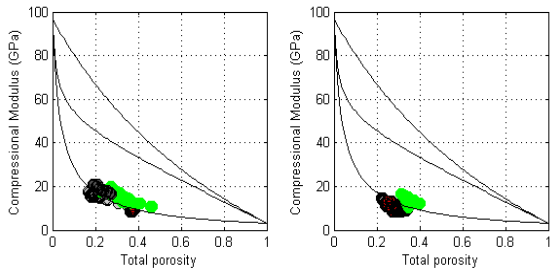

Figure 9. The compressional modulus versus porosity for Well 1 (left) and Well 2 (right). The oil sand is shown in green. The gas sand is red and the shale is gray and black. The bitumen's bulk and shear moduli are 2.50 and 0.50 GPa, respectively.

In addition to the lower Hashin-Shtrikman bound we also show in the same figure the upper Hashin-Shtrikman bound and Hill's average curves. Both strongly overestimate the elastic moduli from the well data.

DOI http://dx.doi.org/10.1190/segam2012-0861.1

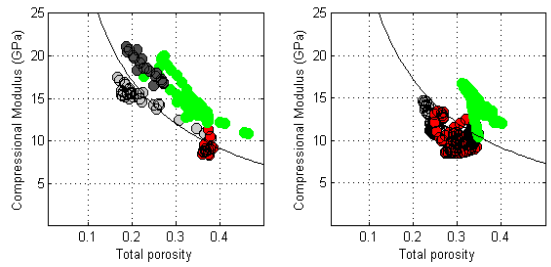

Figure 10. Same as Figure 9 but zoomed on the porosity and elastic modulus intervals of interest.

Next, we repeat the same modeling exercise but now using the bulk and shear moduli of the bitumen according to Batzle et al. (2004), which are 3.50 for the bulk and 0.70 GPa for the shear moduli, respectively. The results are shown in Figure 11 and 12 which are the same as Figures 9 and 10, respectively, but with the theoretical curves computed for the Batzle et al. (2004) elastic properties of the bitumen.

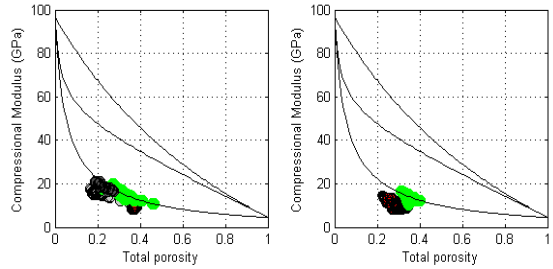

Figure 11. Same as Figure 9 but for the bulk and shear moduli of the bitumen 3.50 and 0.70 GPa, respectively.

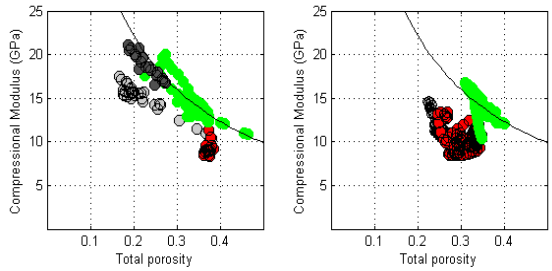

Figure 12. Same as Figure 10 but zoomed on the porosity and elastic modulus intervals of interest.

We observe now that in this case, the oil sand data fall precisely upon the lower Hashin-Shtrikman bound curves simply because these curves plot higher than those computed using the lower elastic moduli of the bitumen.

At this point we do not have exact values for the bitumen properties at the site under examination. This means that the modeling presented here contains sensitivity analysis.

Nevertheless, the lower Hashin-Shtrikman bound appears as a reasonable and physically consistent model for high-porosity bitumen sands where the sand grains are essentially suspended in the bitumen.

Conclusions

Intuitively, the sand grains in high-porosity bitumen sand are suspended in bitumen and, hence, the elastic properties of such sand should be those of a suspension of quartz particles in pure bitumen, described by the lower Hashin-Shtrikman bound.

A number of reasons may violate this assumption. Perhaps the most important reason is that the sand grains are not necessarily perfect spheres and, hence, can have grain-to-grain contacts even at high porosity. Also, the mineralogy may not be 100% quartz and include some other elements. Next, the bitumen filling the grain contacts may be heavier than that in the large pores thus effectively creating grain contact cement.

The effect of direct grain-to-grain contact may be very important for the elastic properties prior to production and especially so during production when the sand compacts and grains move towards each other.

One way of addressing this specific issue is to analyze repeated seismic surveys and, in the best-case scenario, repeated well measurements.

Another way is to conduct computational experiments on true 3D images of oil sand where we may be able to simulate production-related changes by altering the geometry of the virtual rock. The same can be done on idealized granular structures comprised, e.g., by spherical particles.

Such data and computational experiments will help us assess the deviations of the effective elastic moduli from the lower Hashin-Shtrikman bound and relate these deviations to the fabric of the rock and its temporal variations.

In the end, we feel that the rock physics model established here is a robust first-order approximation for real data and can serve as a starting point for developing more advanced theories.

DOI http://dx.doi.org/10.1190/segam2012-0861.1

http://dx.doi.org/10.1190/segam2012-0861.1

EDITED REFERENCES

Note: This reference list is a copy-edited version of the reference list submitted by the author. Reference lists for the 2012 SEG Technical Program Expanded Abstracts have been copy edited so that references provided with the online metadata for each paper will achieve a high degree of linking to cited sources that appear on the Web.

REFERENCES

Batzle, Michael, and De-Hua Han, 2006, Heavy oils — Seismic properties: The Leading Edge, **25**, 750–756.

Das, Agnibha, and Mike Batzle, 2008, Modeling studies of heavy oil — In between solid and fluid properties: The Leading Edge, **27**, 1116–1123.

Mavko, Gary, Tapan Mukerji, and Jack Dvorkin, 2009, The rock physics handbook: Tools for seismic analysis in porous media: Cambridge University Press.

Wolf, Kevin, 2010, Laboratory measurements and reservoir monitoring of bitumen sand reservoirs: Ph.D. dissertation, Stanford University.

DOI http://dx.doi.org/10.1190/segam2012-0861.1